Polaritonic nonlocality in light-matter interaction

Shima Rajabali[1,*], Erika Cortese[2], Mattias Beck[1], Simone De Liberato[2], Jérôme Faist[1], Giacomo Scalari[1,*]

[1]*Quantum Optoelectronics Group, Institute of Quantum Electronics, ETH Zürich, 8093 Zürich, Switzerland*

[2]*School of Physics and Astronomy, University of Southampton, Southampton, SO17 1BJ, United Kingdom*

Sub-wavelength electromagnetic field localization has been central in photonic research in the last decade, allowing to enhance sensing capabilities [1] as well as increasing the coupling between photons and material excitations [2,3]. The strong and ultrastrong light-matter coupling regime in the THz range with split-ring resonators coupled to magnetoplasmons has been widely investigated, achieving successive world-records for the largest light-matter coupling ever achieved [4–7]. Ever shrinking resonators have allowed to approach the regime of few electrons strong coupling [8–10], in which single-dipole properties can be modified by the vacuum field [11]. Here we demonstrate, theoretically and experimentally, the existence of a limit to the possibility of arbitrarily increasing electromagnetic confinement in polaritonic systems. Strongly sub-wavelength fields can excite a continuum of high-momenta propagative magnetoplasmons. This leads to peculiar nonlocal polaritonic effects, as certain polaritonic features disappear and the system enters in the regime of discrete-to-continuum strong coupling[12–14].

Nanophotonic structures confine electromagnetic radiation below the Abbe diffraction limit by storing part of the electromagnetic energy into kinetic energy of moving charges [1]. Primarily relying on metals as charge reservoirs, plasmonics has mainly targeted the visible portion of the electromagnetic spectrum. The possibility to extend the plasmonic excitation to low frequencies (Mid-IR and THz)[15–17] employing semiconductors and two-dimensional systems with tunable plasma frequency through carrier concentration has allowed extreme electromagnetic field confinements in nanostructures [18]. In parallel, ultrastrong light-matter coupling [2,3] has gained recently a lot of attention due to the possibility of observing new quantum phenomena as squeezed vacuum [19] and long-sought superradiant quantum phase transition [20] . Several recent experiments have also allowed to access and measure these squeezed states and their correlation properties[21,22]. Ultrastrong coupling (USC) takes place when the vacuum Rabi frequency (Ω_R), measuring the resonant half-splitting between the lower and upper polariton branches, becomes a considerable fraction (customarily above 10%) of the frequency of the uncoupled systems (ω_0). Semiconductor platforms allow a high degree of control and flexibility and have proven very successful for the study of this physics[19,23,24]. Multiple efforts have been made to scale down the size of photonic resonators [9,25]. This scaling aims to increase the light-matter coupling and reach the regime of few electrons strong coupling in molecular [26] and solid-state devices [27] , where nonlinearities become important and individual electronic degrees of freedom can be manipulated [11,28].

Landau polaritons [4,29] are an experimental platform for light-matter coupling where magnetoplasmons, that are collective electronic excitations, play the role of matter (ultra)-strongly coupled to the near field of electronic (LC) metamaterial photonic resonators. They have been demon-

strated in electron and hole gases [30] confined in semiconductor heterostructures. The strongest achieved couplings ($\frac{\Omega_R}{\omega_0} > 1.4$) make use of metallic split-ring resonators that are able to confine the mm-wave radiation in extremely sub-wavelength volumes [5]. Reducing the capacitor gap in the LC circuit that constitutes the meta-atom has been shown to dramatically enhance the THz fields both for split-ring resonators [31] and non-resonant structures[32,33]. Obtaining the same field enhancement in cavities loaded with active material (i.e., semiconductor quantum wells) requires nevertheless a careful analysis of the different components involved. An important question arises: What are the physical limitations to reducing the cavity volume and subsequent increase of the light-matter coupling? In this work we demonstrate how polaritonic nonlocal effects, consisting in the generation of high-momenta magnetoplasmons by the sub-wavelength resonator, effectively limit the achievable field confinement, and thus the resonant polaritonic splitting. Our theory shows that discrete-to-discrete models underlying the polaritonic framework are not valid anymore below a threshold gap size, as the increased momentum uncertainty due to the spatial electromagnetic confinement couples the discrete cavity mode to a continuum of high-momenta magnetoplasmons. The system then converts to a discrete-to-continuum light-matter coupling model, whose non-perturbative physics has just recently started to be investigated [12–14,34]. Experiments and finite element simulations support this picture, demonstrating multiple novel nonlocal polaritonic features, predicted by the theory. In particular a reduction of the capacitor gap leads to a progressive disappearance of the upper polariton branch and a vanishing contrast below a threshold magnetic field for the lower branch.

Polaritonic Nonlocality

Below critical lengthscales, the propagative nature of charge excitations in nanophotonic devices cannot be neglected anymore, leading to the emergence of nonlocal effects, as demonstrated in both plasmonic [35] and phononic [36] systems. In such a regime the nanoscopic features confining the charge distribution, acting as a grating, allow the electromagnetic field to couple with high-momenta matter resonances. These modes can act as loss channels and reduce the field confinement by smearing the distribution of surface charges, thus ultimately limiting the achievable field enhancement.

In polaritonic systems a different route toward nanoscopic confinement is to use the electromagnetic field itself to define the coupled region out of an extended electronic system, as in metal nanogap resonators fabricated on the top of a two-dimensional electron gas (2DEG) [8]. Beyond the comparative ease of designing and tuning electromagnetic nanoresonators, this procedure also tends to maximise the modal overlap between light and matter modes, having contributed to multiple world-records in the achieved coupling strength [4–6]. In resonator-defined systems nonlocal effects are also eventually bound to play a role. Tightly bound electromagnetic modes have in fact ill-defined momenta, making the standard momentum-space Hopfield approach inapplicable. In non-dispersive systems strong light-matter coupling can still be studied using real-space approaches [37], but when the dispersion becomes non-negligible we are obliged to take into account the coupling of the electromagentic field to a continuum of high-momenta propagative electronic modes.

We developed a polaritonic theory able to study nonlocal effects in an extended electronic system coupled to a photonic nanoresonator, allowing us to understand their impact on the precise engineering of light-matter coupling at the nanoscale. The optical response of a 2DEG in the absence of applied magnetic field can be described in terms of 2D plasma waves indexed by their in-plane momenta $\mathbf{k}$. Their dispersion, shown in the top row of Fig. 1, reads

$$\omega_P(k) \quad = \quad \sqrt{\frac{ke^2\rho_{2DEG}}{2m^*\epsilon_0\epsilon_r}}, \tag{1}$$

where ρ_{2DEG} is the 2DEG density, m^* the electron effective mass, and ϵ_r the background effective dielectric function [38]. A perpendicular magnetic field B with cyclotron frequency ω_c will dress the plasma waves, leading to field-dependent 2D magnetoplasmon resonances whose local non-retarded frequency is $\bar{\omega}_P(k) = \sqrt{\omega_P(k)^2 + \omega_c^2}$ [39]. Note that in this paper the bar over a frequency will be consistently used to indicate magnetically shifted frequency values.

The sub-wavelength nanoresonator breaks the in-plane traslational invariance and the in-plane wavevector $\mathbf{k}$ is thus not a conserved quantity in the light-matter interaction. The photon with frequency ω_0 can thus couple with the continuum of plasma waves occupying the spectral region $\omega > \omega_c$. The strength of the interaction between the photon and plasma waves of frequency $\omega_P(k)$ is given by the coupling density $g(\omega_P(k))$, proportional to the 2D Fourier transform of the electromagnetic field profile in the 2DEG plane. If the smallest geometric feature of the electromagnetic field is of order d, its Fourier transform will have non-vanishing components up to a wavevector value k_d of order $\frac{1}{d}$. The photon will thus couple with plasma waves having, for $B = 0$, maximal frequency $\omega_d = \omega_P(k_d)$. This can be interpreted as a diffraction effect, in which the near-field of the photonic resonator diffracts in the far-field of the plasma waves.

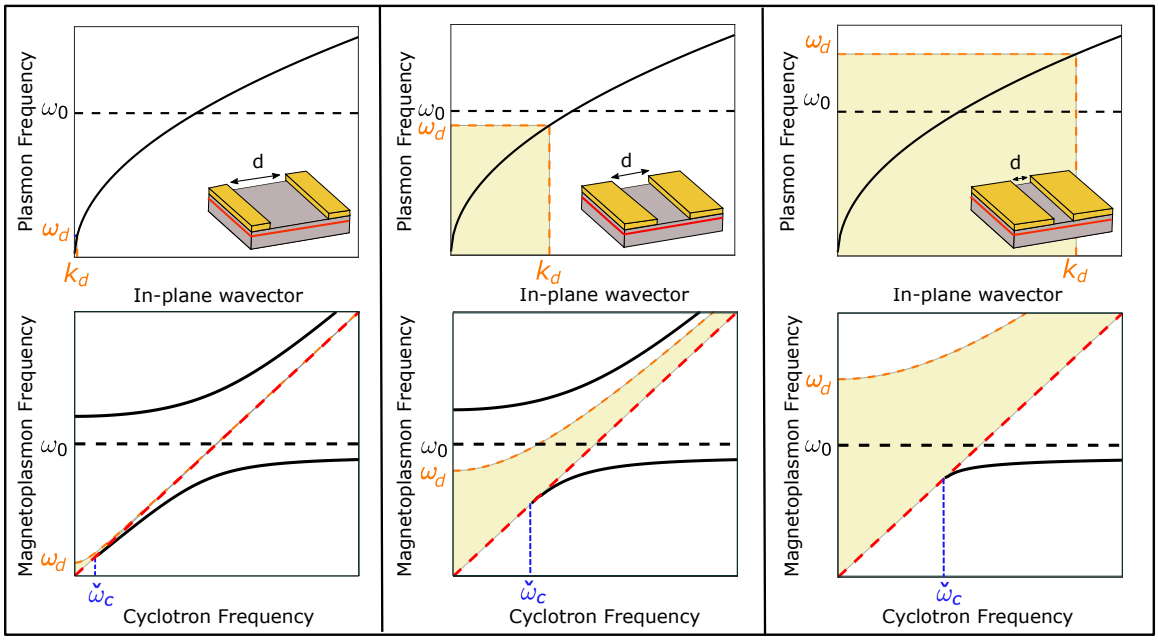

Figure 1: **Impact of nonlocality in nanoplasmonics.** Top row: Dispersion of the bare 2D plasma resonance (i.e., in the absence of the photonic resonator) as a function of the in-plane wavevector. A resonator with features of width d couples with plasma waves with in-plane wavevector up to the value k_d, corresponding to the frequency range shaded, going from 0 to a maximal frequency ω_d at $B = 0$. The horizontal dashed line marks the frequency of the cold cavity, with no 2DEG coupled to the plasmons. Bottom row: Polaritonic resonances, obtained from the coupling between the free plasmonic and photonic modes depicted in the top row, as a function of the cyclotron frequency. The shaded regions between the cyclotron transition ω_c (red dashed line) and the magnetically-shifted edge of the continuum $\bar{\omega}_d = \sqrt{\omega_d^2 + \omega_c^2}$ (orange dashed line) highlight the continuum of possible magnetoplasmonic energies to which the photonic resonator (dashed black line) can couple. The lower polariton merges into the continuum at the critical cyclotron frequency $\check{\omega}_c$. The insets in the top row show a scheme of the nanogap resonator. The position of the 2DEG is marked in red, and the three columns are relative to different nanogap sizes, decreasing toward the right.

The eigenequation of our system can be put in the form

$$\omega^2 - \omega_0^2 = \omega_0 \left[\Delta(\omega) + i\Gamma(\omega)\right], \tag{2}$$

where $\Delta(\omega)$ and $\Gamma(\omega)$ are real functions whose expression can be found in the Methods section. The function $\Gamma(\omega)$ is different from zero only in the region $\omega_c \leq \omega \leq \bar{\omega}_d$, shaded in the second row of Fig. 1. In this spectral interval the frequency of the polaritonic resonances becomes complex, as the continuum of plasma waves irreversibly absorbs photons even neglecting intrinsic plasmonic and photonic losses. The physics is akin to the one found in Landau damping [40], where in our case energy is dissipated generating plasma waves and not free electron-hole pairs.

While in a standard Landau polariton model [7] the two polaritonic branches exist for any value of the magnetic field, when ω_d becomes non-negligible the extreme photonic confinement can dramatically change the nature of the light-matter system as the narrow polaritonic resonances broaden and vanish into the continuum region. An analysis of the solutions of Eq. 2 shows the existence of a critical cyclotron frequency $\breve{\omega}_c$ such that a narrow lower polariton exists only for $\omega_c > \breve{\omega}_c$. A narrow upper polariton instead exists if $\omega_0 > \bar{\omega}_d$, implying that the upper polariton region is outside of the continuum, or if the coupling $g(\omega)$ is large enough to push the discrete resonance out of the continuum, analogously to the case studied in Ref. [13] for the lower edge of the ionization continuum.

The physics described is sketched in Fig. 1. In the left column ($\omega_d, \breve{\omega}_c \approx 0$) the two polaritonic resonances are visible for most values of B, while in the central one ($\omega_d < \omega_0$) the upper polariton is still present but the lower polariton disappears for $\omega_c < \breve{\omega}_c$. For even smaller nanores-

onators ($\omega_d > \omega_0$) also the upper polariton disappears, as shown in the right column.

Experimental Results

We now proceed to the experimental study where we measure a 2DEG coupled to a metasurface of complementary split-ring resonators (cSRR)s in a series of samples where we vary the central gap width d, from 4 μm down to 250 nm (complete sample layout in Supplementary Info: "Supporting experimental measurements" and Fig. S1). A scanning electron microscope (SEM) picture of one unit cell of the metasurface is shown in Fig. 2a. The electric field polarization direction used in the experiments to excite the LC mode of the resonator is perpendicular to the gap of the resonator (red arrow in Fig. 2b).

In the cold cavity case (no 2DEG present), the electric field of the cSRRs' fundamental mode is concentrated in the central gap for any value of the gap d and its modal volume will scale as $V = L_{Gap} \times d \times L_{eff}$, where L_{eff} is the effective penetration depth of the fringing field inside the substrate (Fig. 2c). Note that, as the central gap acts as a capacitor in the LC split-ring circuit, it directly affects the resonant frequency of the resonator $\omega_0 = 2\pi f_{LC} = \frac{2\pi}{\sqrt{LC}}$. In order to allow for a meaningful comparison between different samples we thus re-scaled the resonators in order to keep a fixed cSRR frequency at $f_{LC} = 500$GHz. Only the electrons within a cavity effective surface S of order $L_{Gap} \times d$ will couple to the strong TE electric field of the resonator's LC mode, leading to a total effective electron number $N_{2DEG} = \rho_{2DEG} S$. The vacuum Rabi frequency $\Omega_R \propto \sqrt{\frac{N_{2DEG}}{V}}$, quantifying resonant coupling of a discrete photonic mode to a single magnetoplasmon resonance,

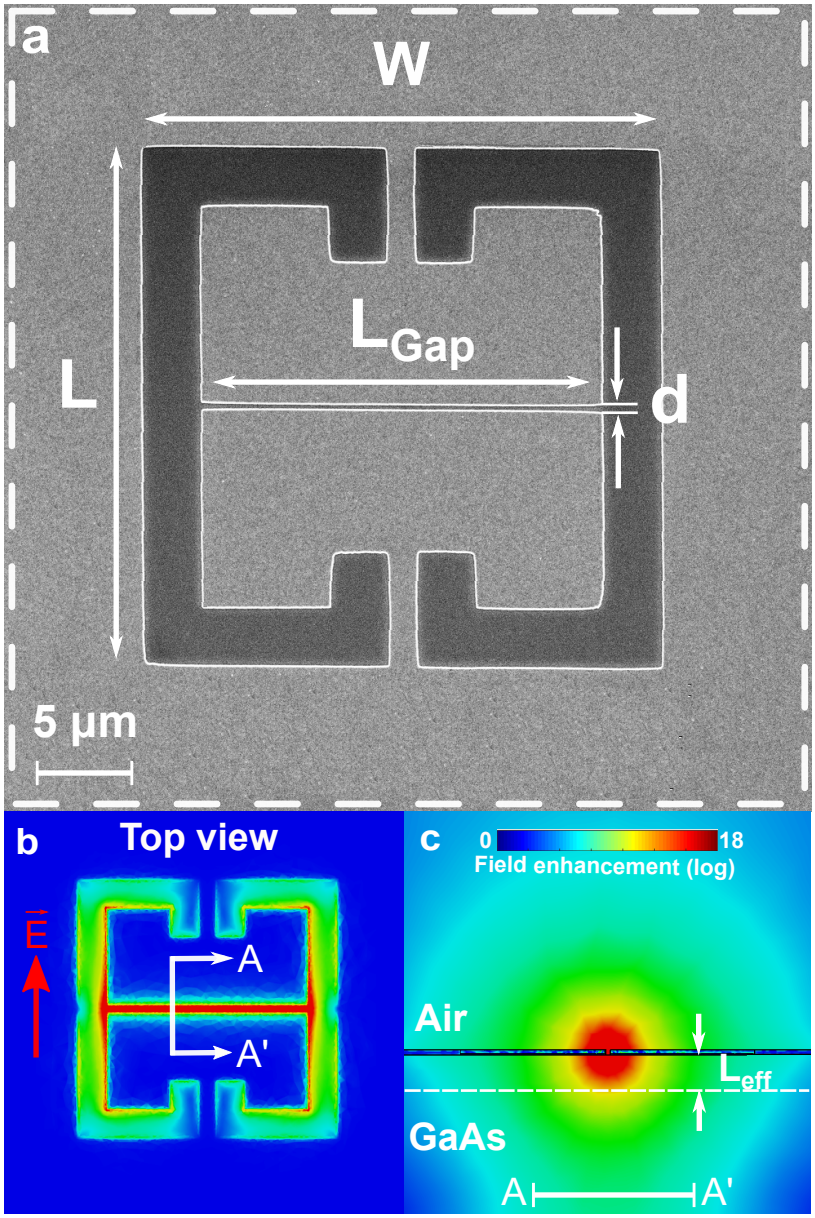

Figure 2: **Cavity and electric field parameters** (a) A SEM image of a unit cell (white dashed line square) containing a cSRR with 250 nm gap showing different resonator parameters including gap size d. (b,c) Cold cavity electric field distribution for the electric field polarization direction perpendicular to the gap (red arrow), simulated by CST, for cSRRs resonating at 500 GHz in two different views: Top view (b) and AA' view or yz plane (c). You can find L_{eff} in panel (c). (b) and (c) have the same colorbar.

can then be explicitly written as

$$\Omega_R = \sqrt{\frac{e^2 \rho_{2DEG}}{4m^* \epsilon_0 \epsilon_r L_{eff}}}. \tag{3}$$

Although the explicit dependence of the coupling upon the gap width d cancels in Eq. 3, L_{eff} changes due to the reduced d dimension. This dependency is borne out by our finite element electromagnetic simulations for the cold cavity case, where there is no 2DEG underneath the metallic surface, showing a more confined and enhanced electric field in a narrower gap (Fig. S4 in Supplementary info). Reducing the gap size d is thus expected to increase the coupling Ω_R for a fixed cavity frequency [6].

The sample transmission is measured using THz time-domain spectroscopy (TDS) at temperature T = 2.7 K as a function of an external out of plane magnetic field swept between 0 and 4 T. In the top row of Fig. 3a we report the experimental results. The colormap corresponding to $d = 4$ μm gap size ($\omega_0 \gg \omega_d$) shows an anti-crossing of the first cavity mode with the linear cyclotron transition dispersion at an out plane magnetic field $B \approx 1.2$T. The solid black lines show the lower polariton and upper polariton branches fitted to the extracted maximum of transmission using our theory in the discrete-to-discrete regime, equivalent to the standard Hopfield model [4,7]. For the resonator with d=750 nm ($\omega_0 > \omega_d$) we observe a broadening of the UP branch but we can still extract the maximum of the transmission at each magnetic field. We plot the the normalized coupling ratio $\frac{\Omega_R}{\omega_0}$ extracted from a theoretical fit of the data for $d > 750$nm, where the nonlocal effects discussed above are not relevant and the system is well described by a standard single mode Hopfield model (Fig. 3b). In such a regime we can extract a $\frac{1}{\sqrt{d}}$ dependence of the normalized

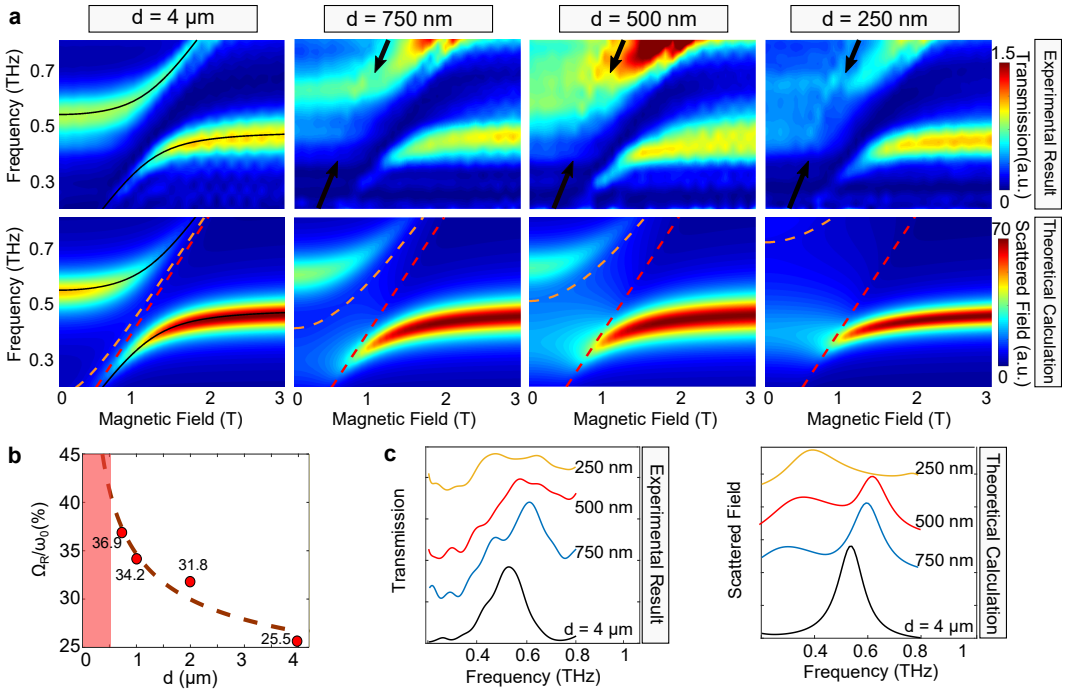

Figure 3: **Theoretical vs. Experimental results** (a) Top row: transmission of cSRRs coupled to Landau level transition in 2DEG vs. magnetic field for four different gap sizes d. Bottom row: the calculated scattered Field for a gap feature size of d, same as gap sizes in experiment result. The black solid lines are fitted LP and UP. The black arrows show an additional feature corresponds to $f = 1.6 \times \omega_c/2\pi$. The regions between the cyclotron transition ω_c (red dashed line) and the magnetically-shifted continuum edge $\bar{\omega}_d$ (orange dashed line) are similar to shaded regions on the bottom row of Fig. 1, showing the region of continuum magnetoplasmon energies. The slight changes in linewidth of the LP at its asymptotic limit are below the accuracy of our measurement setup and do not have a physical interpretation. (b) Normalized coupling vs. d. Dashed brown line indicates the predicted dependence of $\frac{\Omega}{\omega}$ on $\frac{1}{\sqrt{d}}$. The red region corresponds to gap values < 600 nm where the large broadening of the upper branch does not allow a measurement of the coupling. (c) Sections (offset for clarity) of the color plots at zero magnetic field for experimental result and theoretical calculation in panel (a). The progressive upper branch broadening is evident.

coupling over the gap width (dashed brown line). For 500 nm ($\omega_0 \approx \omega_d$) and especially for 250 nm ($\omega_0 < \omega_d$) gap sizes the upper branch does not display a clear maximum anymore and the signal is broadened over a frequency range of over 200 GHz. Our optical measurements probe the photonic part of the polaritonic excitations, which for the lower branch naturally vanishes when $B \to 0$. This effect makes it difficult to highlight the lower polariton disappearance at finite values of the magnetic field predicted by our theory. Inspection of 3a nevertheless shown a clear reduction of the lower branch visibility range for the smallest gap.

In order to better compare to experimental results, Fig. 3a (bottom row) plots theoretical calculation results obtained including losses affecting both the photonic and magnetoplasmon fields. As detailed in the Methods section, this has been accomplished extending the dissipative diagonalization procedure for cavity quantum electrodynamics (CQED) from Ref. [12]. The cyclotron transition ω_c (red dashed line) and the magnetically-shifted continuum edge $\bar{\omega}_d = \sqrt{\omega_d^2 + \omega_c^2}$ (orange dashed line) bound the region of continuum magnetoplasmon energies shaded in Fig. 1 and they visualize the loss channel leading the broadening of the upper polariton branch in our transmission data.

The enhanced transmission visible at higher frequencies in the experimental data is due to the second mode of the cSRRs lying close to 1THz. This mode is not strongly confined in the gap and it is not relevant for the nonlocal physics of the system. It has thus not been included in the theoretical modeling. To clearly illustrate the upper polariton broadening, sections of all four color plots for both experimental and theoretical results in Fig. 3a at zero magnetic field are plotted in Fig. 3c. The progressive broadening of the upper polariton branch is manifest. The clear blue shift of the

upper polariton from 4 μm to 750 nm gap at zero magnetic field is related to the opening of the polariton gap [24], another indication of larger coupling strength in cSRRs with small slits [6].

The experimental transmission measurements display also linear dispersions appearing for the smallest gaps (indicated by black arrows in Fig. 3a). Such linear dispersions correspond to optical transitions at multiples of the cyclotron frequency. In a two dimensional electron gas the cyclotron resonance frequency should not depend on the carrier density as the radiation couples only to the center-of-mass motion of the electron system. This very general result, known as Kohn's theorem [41], is strictly valid for parabolic bands and translationally invariant systems. Here we observe indeed a breaking of such theorem due to the presence of a spatially modulated charge density (the magnetoplasmon) that leads to a breaking of the translational invariance. The lack of translational invariance leads to a relaxation of the optical selection rules between Landau levels allowing the observation of transitions at multiples of the cyclotron frequency. Such effect has been already observed experimentally in the case of magnetoplasmons coupled to cyclotron resonance [42] [38] but never in the context of Landau polaritons, where the momentum matching element is part of an optical cavity. In this case the observed effect is again arising due to the diffraction emerging with the introduction of very narrow resonator gaps.

3D finite element electromagnetic simulations

In order to quantitatively confirm the theoretical predictions using the detailed cSRR geometry and visualize the nonlocal coupling to 2D magnetoplasmon modes, we recurred to finite element elec-

tromagnetic simulation (CST Microwave Studio) in which the 2DEG is modeled as a gyrotropic material. No "effective medium" is adopted, i.e., the dimensions of the different components including the thickness of the quantum well layer (10 nm) are kept as in reality. The 2DEG electron density used in the simulation is calibrated by matching the cyclotron absorption strength with measurements performed on the bare (no cavity) heterostructure used in the experiment. A full description of the model and the employed parameters can be found in supplementary document ("Supporting numerical simulations" and Fig. S5).

A set of simulation of the Landau polariton dispersion for the metallic metasurface with a gap of 250 nm deposited on 2DEG as a function of magnetic field is reported in Fig. 4a. In this simulation, magnetic field is swept in the range $B \in [0, 4]$ T, and can be directly compared with the corresponding experimental plot of Fig. 3a. As visible, the finite element simulation reproduces very well the broadening of the upper polariton branch. It is interesting to inspect the electric field distribution at the anti-crossing (white dashed line in Fig. 4a). As visible from Fig. 4d the upper branch, expected to sit in the magnetoplasmon continuum, is completely dominated by the propagative plasmonic behavior and the corresponding peak is largely broadened. Conversely, the lower branch (Fig. 4c) displays the electric field intensity all concentrated in the gap. More simulation data on broadening of UP and partially disappearance of the LP can be found in the Supplementary info (Fig. S6-S9).

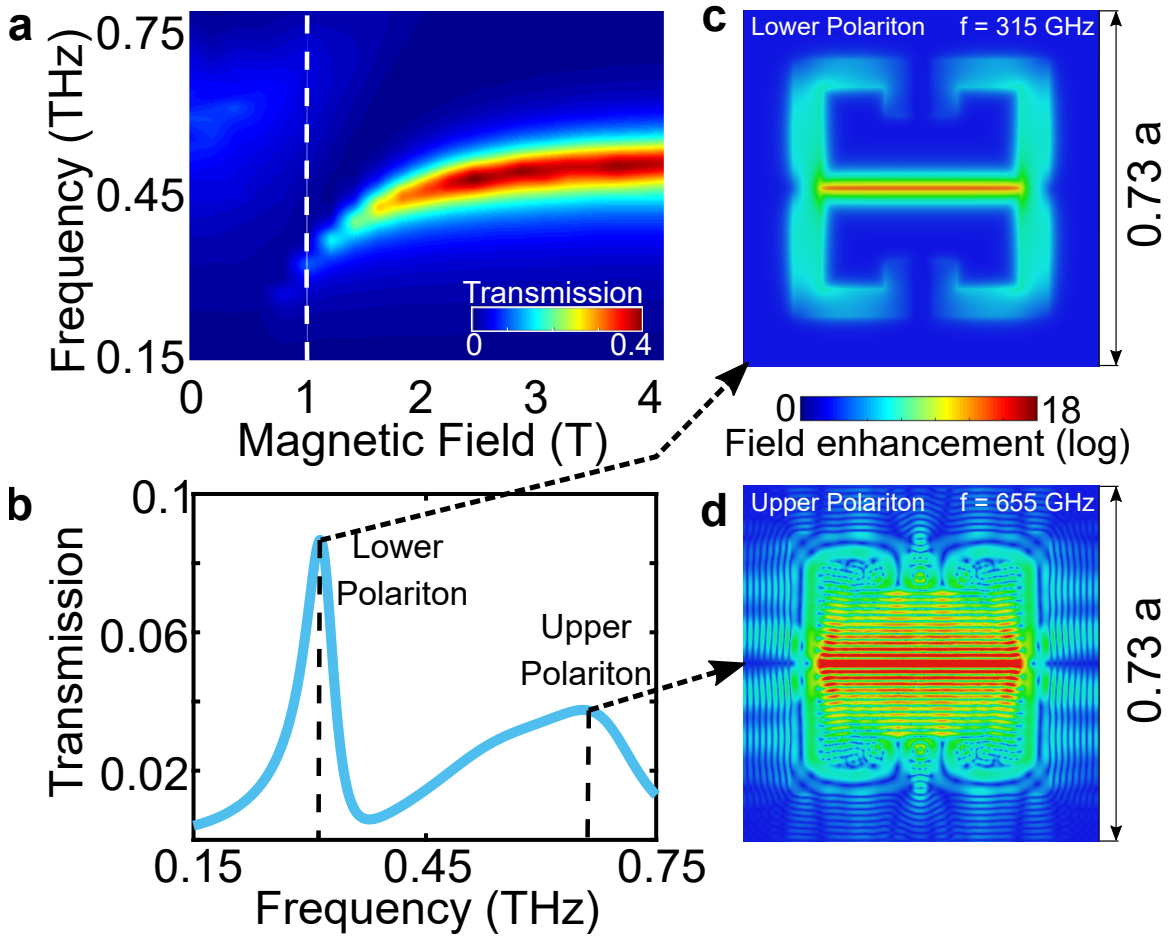

Figure 4: **Finite element simulation for cSRR with 250nm gap on 2DEG** (a) Simulation of the Landau polariton dispersion as a function of magnetic field. The broadening and loss of contrast of the upper branch is evident in (b), section of the color plot of panel (a) at the anti-crossing field B = 1T. In panels (c) and (d) we report the electric field distributions for UP and LP. The field distribution in (c) for LP shows a pronounced electric field concentration in the 250 nm gap and a corresponding narrow spectral distribution. On the other side, panel (d) clearly demonstrates the excitation of plasmonic standing waves and the corresponding peak in the frequency spectrum is broad.

Conclusions

In conclusion, we theoretically investigated the emergence of nonlocality in polaritonics. Contrary to nonlocality in plasmonic [35] and phononic [36] systems, caused by tight charge confinement, here nonlocal effects are driven by the confinement of the resonator's electromagnetic field coupling to a continuum of propagating magnetoplasma excitations. We experimentally observed such a physics using Landau polaritons at sub-THz frequencies employing nanometer-sized resonators. First, we show that when nonlocal effects are not relevant (gap size $d > 750$ nm) the normalized coupling ratio between light and matter scales as $\frac{1}{\sqrt{d}}$, increasing by about 50% from $d = 4\mu$m to 750 nm, and reaching 37% for a single quantum well due to the strong field enhancement. For smaller gap values, nonlocal effects become dominant and the system is not anymore well described by a standard Hopfield model. As predicted by our multimode dissipative bosonic Hamiltonian we observe a broadening of the upper polariton branch and the partial disappearance on the lower one. Finite element electromagnetic simulations confirm this interpretation. The presence of highly localized electric fields is as well testified by the presence of features related to breaking of Kohn's theorem. Our findings set quantitative limits to the miniaturization of polaritonic devices, and to the enhancement of polariton gaps, as well as open new possibilities in the study of discrete-to-continuum strongly coupled systems [12–14].

Methods

Theoretical description of light-matter coupling. We model the magnetoplasmonic excitations coupled to a single photonic mode using a generalisation of the multimode Hamiltonian developed in Ref. [13]

$$H = \hbar\tilde{\omega}_0 a^\dagger a + \sum_{\mathbf{k}} \hbar\bar{\omega}_P(k)\, b^\dagger_{\mathbf{k}} b_{\mathbf{k}} + i\hbar\Omega_R \sum_{\mathbf{k}} \sqrt{\frac{\bar{\omega}_P(k)}{\tilde{\omega}_0}} \left[a^\dagger + a\right] \left[\Xi_{\mathbf{k}} b_{\mathbf{k}} - \Xi^*_{\mathbf{k}} b^\dagger_{\mathbf{k}}\right], \qquad (4)$$

where a is the annihilation operator for a resonator photon and $b_{\mathbf{k}}$ annihilates a magnetoplasma wave with in-plane wavevector $\mathbf{k} = (k_x, k_y)$ and bare ($\omega_c = 0$) frequency $\omega_P(k)$. The second-quantised operators obey bosonic commutation relations $\left[a, a^\dagger\right] = 1$ and $\left[b_{\mathbf{k}}, b^\dagger_{\mathbf{k}'}\right] = \delta_{\mathbf{k},\mathbf{k}'}$, where the δ is a Kronecker symbol. The Heisenberg equations generated by Eq. 4 are linear in the creation and annihilation operators, and such a quantum theory is thus equivalent to a semiclassical dielectric approach when the system is excited with classical light as in our experiments. The quantum approach is nevertheless able to model also purely quantum results, when the polaritons are excited with non-classical light [43]. As better detailed in the Supplementary info, the photonic frequency $\tilde{\omega}_0$ includes the renormalisation due to the diamagnetic A^2 term in the Hamiltonian, while $\bar{\omega}_P(k)$ is the magnetoplasmon frequency. In Eq. 4 the vacuum Rabi Frequency Ω_R is given by Eq. 3 and $\Xi_{\mathbf{k}}$ is the 2D Fourier transform of the resonator field in the 2DEG plane. The explicit derivation of these quantities can be found in the Supplementary info. Note that the Hamiltonian in Eq. 4 is not in the usual form found in polaritonic problems, where a dispersionless matter excitation (e.g., TO phonons in bulk) couples to a dispersive electromagnetic mode. In such a case both light and matter have in-fact the same spatial symmetry, and momentum conservation

enforces a one-to-one coupling between light and matter modes. The model in Eq. 4 describes instead a one-to-many coupling, formally more similar to models used to describe losses in an open quantum system. In the continuum regime the Hamiltonian in Eq. 4 can be rewritten

$$H = \hbar\tilde{\omega}_0 a^\dagger a + \int_0^\infty d\omega\, \hbar\bar{\omega}\, b(\omega)^\dagger b(\omega) + i\hbar \int_0^\infty d\omega \sqrt{\frac{\bar{\omega}}{\tilde{\omega}_0}} \left[a^\dagger + a\right] \left[g(\omega)b(\omega) - g(\omega)^* b(\omega)^\dagger\right], \tag{5}$$

with $\left[b(\omega), b(\omega')^\dagger\right] = \delta(\omega - \omega')$, and the δ is now the Dirac function. The secular equation of the Hamiltonian in Eq. 5 is shown in Eq. 2, with

$$\Delta(\omega) = \frac{4\omega^2}{\omega_0} P \int_0^\infty d\omega' \frac{|g(\omega')|^2}{\omega^2 - \omega'^2 - \omega_c^2}, \tag{6}$$

$$\Gamma(\omega) = \frac{2\pi\omega^2}{\omega_0} \frac{|g(\sqrt{\omega^2 - \omega_c^2})|^2}{\sqrt{\omega^2 - \omega_c^2}} \Theta(\omega - \omega_c), \tag{7}$$

where P is the principal part and $\Theta(\omega)$ the Heaviside function. The minimal cyclotron frequency required for the existence of the lower polaritons $\breve{\omega}_c$ can be obtained by writing Eq. 2 for $\omega = \omega_c$, and solving for the critical value of the cyclotron frequency for which the lower polariton merges into the continuum

$$\breve{\omega}_c = \omega_0 \left[1 + 4P \int_0^\infty d\omega' \frac{|g(\omega')|^2}{\omega'^2}\right]^{-\frac{1}{2}}. \tag{8}$$

Analytical conditions for the existence of the upper polariton could be analogously determined, although they are of limited interest being strongly dependent on the details of the specific resonator geometry. This asymmetry between the two polariton branches is due to the fact that the lower bound of the continuum, ω_c, marks the existence of the plasma waves, while the upper bound, ω_d, is more fuzzy, depending on the Fourier transform of the field profile, which doesn't necessarily presents a well-defined sharp cutoff in $\mathbf{k}$ space.

Theoretical description of the open system In order to better predict experimental features due to nonlocal nanopolaritonic effects, we need to consider the impact of intrinsic polariton losses, due to the finite lifetime of both the cavity photon and the magnetoplasmon. We used to this aim the approach initially introduced by Huttner and Barnett to quantise the electromagnetic field in bulk dissipative dielectrics [44] and recently extended to the CQED case with both material and photonic losses [12]. This approach allows us to to write the system Hamiltonian in terms of a continuum of broadened photonic and magnetoplasmonic modes, with annihilation operators $A(\omega)$ and $B(\omega)$,

$$\begin{aligned} H_{\text{tot}} &= \int_0^\infty \hbar\omega A^\dagger(\omega)A(\omega) + \int_0^\infty \hbar\omega B^\dagger(\omega)B(\omega) \\ &+\hbar\int_0^\infty d\omega \int_0^\infty d\omega' \left[\zeta(\omega)A^\dagger(\omega) + \zeta^*(\omega)A(\omega)\right] \times \left[\theta(\omega')B^\dagger(\omega') + \theta^*(\omega')B(\omega')\right], \end{aligned} \tag{9}$$

satisfying bosonic commutation relations $\left[A(\omega), A(\omega')^\dagger\right] = \left[B(\omega), B(\omega')^\dagger\right] = \delta(\omega - \omega')$. In the Hamiltonian above the function $\zeta(\omega)$ contains the information about the photonic losses, and $\theta(\omega)$ contains a convolution integral between the resonant coupling density $g(\omega)$ and a function describing the frequency-dependent matter losses.

The Hamiltonian in Eq. 9 is then diagonalised by introducing operators for two orthogonal polariton branches $j = \pm$, obeying Bosonic commutation relations $[P_j(\omega), P_{j'}(\omega')] = \delta(\omega - \omega')\delta_{j,j'}$, which we write in terms of the bare broadened fields

$$P_j(\omega) = \int_0^\infty d\omega' \left[x_j(\omega,\omega')A(\omega') + z_j(\omega,\omega')A^\dagger(\omega') + y_j(\omega,\omega')B(\omega') + w_j(\omega,\omega')B^\dagger(\omega')\right]. \tag{10}$$

The frequency dependent Hopfield coefficients (x_j, z_j, y_j, w_j) can then be found by solving the equations of motion $\omega P_j(\omega) = \frac{1}{\hbar}\left[P_j(\omega), H_{\text{tot}}\right]$.

As shown in Ref. [12] such a description is defined modulo a real function of ω, fixing the basis used to specify the two degenerate modes $P_{\pm}(\omega)$. The two polaritonic operators are thus not individually identifiable with the two polaritonic branches, and the observable results have to be calculated from the gauge-invariant bare electromagnetic mode

$$(a + a^{\dagger}) \;=\; \int_0^{\infty} d\omega \sum_{j=\pm} M_j(\omega) \left[P_j(\omega) + P_j^{\dagger}(\omega) \right], \tag{11}$$

with M_j the electric component of the polaritonic field obtained inverting the Hopfield transformation.

Numerical results are obtained assuming that the only relevant scattering feature is across the x axis, and it couples the photon resonator with plasma waves with wavevector up to the value $k_d = \frac{1}{d}$. We can then write $\Xi_{\mathbf{k}} = \Theta(k_d - |k_x|)\delta_{k_y,0}$, with Θ the Heaviside function, leading to a resonant coupling density of the form

$$g(\omega) \;=\; \Omega_R \sqrt{\frac{2\omega}{\pi \omega_d^2}} \Theta(\omega_d - \omega). \tag{12}$$

Sample fabrication, measurement setup, and simulated structure in CST This part is available in Supplementary info.

Data Availability Statement The numerical simulation and measurement data that support the plots within this paper are available from the corresponding author upon reasonable request.

Code availability statement The codes used in the theory part of this study are available from the corresponding author upon reasonable request.

1. Khurgin, J., Tsai, W.-Y., Tsai, D. P. & Sun, G. Landau damping and limit to field confinement and enhancement in plasmonic dimers. *ACS Photonics* **4**, 2871–2880 (2017).

2. Forn-Díaz, P., Lamata, L., Rico, E., Kono, J. & Solano, E. Ultrastrong coupling regimes of light-matter interaction. *Rev. Mod. Phys.* **91**, 025005 (2019).

3. Frisk Kockum, A., Miranowicz, A., De Liberato, S., Savasta, S. & Nori, F. Ultrastrong coupling between light and matter. *Nature Reviews Physics* **1**, 19–40 (2019).

4. Scalari, G. *et al.* Ultrastrong coupling of the cyclotron transition of a 2d electron gas to a thz metamaterial. *Science* **335**, 1323–1326 (2012).

5. Bayer, A. *et al.* Terahertz light-matter interaction beyond unity coupling strength. *Nano Letters* **17**, 6340–6344 (2017).

6. Maissen, C. *et al.* Ultrastrong coupling in the near field of complementary split-ring resonators. *Phys. Rev. B* **90**, 205309 (2014).

7. Hagenmüller, D., De Liberato, S. & Ciuti, C. Ultrastrong coupling between a cavity resonator and the cyclotron transition of a two-dimensional electron gas in the case of an integer filling factor. *Phys. Rev. B* **81**, 235303 (2010).

8. Keller, J. *et al.* Few-electron ultrastrong light-matter coupling at 300 ghz with nanogap hybrid lc microcavities. *Nano Letters* **17**, 7410–7415 (2017).

9. Ballarini, D. & De Liberato, S. Polaritonics: from microcavities to sub-wavelength confinement. *Nanophotonics* **8**, 641–654 (2019).

10. Jeannin, M. *et al.* Ultrastrong light-matter coupling in deeply subwavelength thz lc resonators. *ACS Photonics* **6**, 1207–1215 (2019). arXiv:https://doi.org/10.1021/acsphotonics.8b01778.

11. Ćwik, J. A., Kirton, P., De Liberato, S. & Keeling, J. Excitonic spectral features in strongly coupled organic polaritons. *Phys. Rev. A* **93**, 033840 (2016).

12. De Liberato, S. Virtual photons in the ground state of a dissipative system. *Nature communications* **8**, 1–6 (2017).

13. Cortese, E., Carusotto, I., Colombelli, R. & De Liberato, S. Strong coupling of ionizing transitions. *Optica* **6**, 354–361 (2019).

14. Cortese, E. *et al.* Excitons bound by photon exchange. *Nature Physics* 1–5 (2020).

15. Stanley, R. Plasmonics in the mid-infrared. *Nature Photonics* **6**, 409–411 (2012).

16. Taliercio, T. & Biagioni, P. Semiconductor infrared plasmonics. *Nanophotonics* **8**, 949–990 (2019).

17. Xueqian Zhang *et al.* Terahertz surface plasmonic waves: a review. *Advanced Photonics* **2**, 014001 (19 pp.) (2020).

18. Fei, Z. *et al.* Gate-tuning of graphene plasmons revealed by infrared nano-imaging. *Nature* **487**, 82–85 (2012).

19. Ciuti, C., Bastard, G. & Carusotto, I. Quantum vacuum properties of the intersubband cavity polariton field. *Phys. Rev. B* **72**, 115303 (2005).

20. Nataf, P. & Ciuti, C. No-go theorem for superradiant quantum phase transitions in cavity QED and counter-example in circuit QED. *Nature Communications* **1** (2010).

21. Riek, C. *et al.* Direct sampling of electric-field vacuum fluctuations. *Science* **350**, 420–423 (2015).

22. Benea-Chelmus, I.-C., Settembrini, F. F., Scalari, G. & Faist, J. Electric field correlation measurements on the electromagnetic vacuum state. *Nature* **568**, 202–206 (2019).

23. Anappara, A. A. *et al.* Signatures of the ultrastrong light-matter coupling regime. *Phys. Rev. B* **79**, 201303 (2009).

24. Todorov, Y. *et al.* Ultrastrong light-matter coupling regime with polariton dots. *Phys. Rev. Lett.* **105**, 196402 (2010).

25. Maissen, C., Scalari, G., Beck, M. & Faist, J. Asymmetry in polariton dispersion as function of light and matter frequencies in the ultrastrong coupling regime. *New Journal of Physics* **19**, 043022 (2017).

26. Chikkaraddy, R. *et al.* Single-molecule strong coupling at room temperature in plasmonic nanocavities. *Nature* **535**, 127–130 (2016).

27. Reithmaier, J. P. *et al.* Strong coupling in a single quantum dot–semiconductor microcavity system. *Nature* **432**, 197–200 (2004).

28. Todorov, Y. & Sirtori, C. Few-electron ultrastrong light-matter coupling in a quantum lc circuit. *Phys. Rev. X* **4**, 041031 (2014).

29. Paravicini-Bagliani, G. L. *et al.* Magneto-transport controlled by landau polariton states. *Nature Physics* **15**, 186–190 (2019).

30. Keller, J. *et al.* Landau polaritons in highly nonparabolic two-dimensional gases in the ultrastrong coupling regime. *Phys. Rev. B* **101**, 075301 (2020).

31. Bagiante, S., Enderli, F., Fabianska, J., Sigg, H. & Feurer, T. Giant Electric Field Enhancement in Split Ring Resonators Featuring Nanometer-Sized Gaps. *Scientific Reports* **5** (2015).

32. Chen, X. *et al.* Squeezing Millimeter Waves through a Single, Nanometer-wide, Centimeter-long Slit. *Scientific Reports* **4** (2014).

33. Bahk, Y.-M. *et al.* Ultimate terahertz field enhancement of single nanoslits. *Phys. Rev. B* **95**, 075424 (2017).

34. Forn-Díaz, P. *et al.* Ultrastrong coupling of a single artificial atom to an electromagnetic continuum in the nonperturbative regime. *Nature Physics* **13**, 39–43 (2017).

35. Ciracì, C. *et al.* Probing the ultimate limits of plasmonic enhancement. *Science* **337**, 1072–1074 (2012).

36. Gubbin, C. R. & De Liberato, S. Optical nonlocality in polar dielectrics. *Phys. Rev. X* **10**, 021027 (2020).

37. Gubbin, C. R., Maier, S. A. & De Liberato, S. Real-space hopfield diagonalization of inhomogeneous dispersive media. *Phys. Rev. B* **94**, 205301 (2016).

355 38. Batke, E., Heitmann, D. & Tu, C. W. Plasmon and magnetoplasmon excitation in two-
356 dimensional electron space-charge layers on gaas. *Phys. Rev. B* **34**, 6951–6960 (1986).

357 39. Jin, D. *et al.* Topological magnetoplasmon. *Nat Commun* **7**, 13486 (2016).

358 40. Khurgin, J. B. Ultimate limit of field confinement by surface plasmon polaritons. *Faraday*
359 *Discuss.* **178**, 109–122 (2015).

360 41. Kohn, W. Cyclotron resonance and de haas-van alphen oscillations of an interacting electron
361 gas. *Phys. Rev.* **123**, 1242–1244 (1961).

362 42. Batke, E., Heitmann, D. & Kotthaus, J. P. Non-locality in the two-dimensional plasmon dis-
363 persion. *Physical Review Letters* **54**, 2367 (1985).

364 43. López Carreño, J. C., Sánchez Muñoz, C., Sanvitto, D., del Valle, E. & Laussy, F. P. Exciting
365 polaritons with quantum light. *Phys. Rev. Lett.* **115**, 196402 (2015).

366 44. Huttner, B. & Barnett, S. M. Quantization of the electromagnetic field in dielectrics. *Physical*
367 *Review A* **46**, 4306 (1992).

368 **Acknowledgements** G.S., J.F. and S.R. would like to thank J. Keller for help in the initial phase of the
369 project. G.S. also thanks M. Jeannin and R. Colombelli for discussions. S.R. thanks I.-C. Benea-Chelmus
370 for fruitful discussions. G.S. and J.F. acknowledge financial support from the ERC Advanced grant Quantum
371 Metamaterials in the Ultra Strong Coupling Regime (MUSiC) with the ERC Grant 340975. G.S. and J.F.
372 also acknowledge financial support from the Swiss National Science Foundation (SNF) through the National
373 Centre of Competence in Research Quantum Science and Technology (NCCR QSIT). S.D.L. is a Royal

Society Research Fellow and was partly funded by the Philip Leverhulme Prize of the Leverhulme Trust. E.C. acknowledges funding from the RGF\EA\181001 grant of the Royal Society.

Competing Interests The authors declare that they have no competing financial interests.

Authors contributions G.S., J.F. and S.D.L. conceived the idea. S.R. designed and fabricated the devices, and carried out all the optical measurements, analysed all experimental data and performed numerical simulations under the supervision of G.S. and J.F.. E.C. and S.D.L. developed the theory. M.B. performed the epitaxial growth. S.R., S.D.L. and G.S. wrote the manuscript. All authors discussed the results and commented on the manuscript.

Correspondence *Correspondence should be addressed to S. Rajabali (email: shimar@phys.ethz.ch) and G. Scalari (email: scalari@phys.ethz.ch) and S. De Liberato (s.de-liberato@soton.ac.uk).